

Simultaneous Optical to X-ray Spectra of OJ 287: Insights into X-ray spectral changes and particle spectra

Pankaj Kushwaha^[0000–0001–6890–2236]

Abstract OJ 287 is one of the most dynamic BL Lacertae objects that has exhibited behaviour representative of the entire blazar class and is also one of the best sources with simultaneous multi-wavelength coordinated data. Motivated by strong X-ray variability exhibited by the source, we systematically investigated the simultaneous optical to X-ray emission of the source with a focus on the spectral state of the lowest recorded X-ray flux state to understand the X-ray spectral changes. The optical-UV emission being synchrotron, the associated spectral variation is a direct reflection of the high-energy end of the underlying particle spectrum and its power-law continuation to X-rays can drastically affect the X-ray spectrum without much change in optical flux. Thus the combined optical to X-ray provides a potential tool to investigate and explore particle spectrum as well as highest particle energies. We report the finding of a power-law optical-UV spectrum with a photon spectral index of 2.71 ± 0.03 continuing to X-ray energies and accounting for this contribution at X-ray results in a photon spectral index of $1.15 - 1.3$. We discuss the possible implications of this on X-ray spectral variations and the particle spectrum.

1 Introduction

Accretion-powered sources are the most dynamic astronomical sources in the sky exhibiting frequent and often drastic changes in their observational behaviour, especially the compact systems. The observed behaviour and properties of the latter imply a significant contribution from relativistic species,

Pankaj Kushwaha

Department of Physical Sciences, Indian Institute of Science Education and Research Mohali, Knowledge City, Sector 81, SAS Nagar 140306, India e-mail: pankaj.kushwaha@iisermohali.ac.in

generally in the form of non-thermal components. Studies exploiting different approaches to investigate these sources indicate quite broad similarities in some of the observational properties (e.g. temporal: [1, 2, 3, 4, 5], and references therein) while completely contrary in other properties (e.g. spectral: [6] and references therein), implying a very diverse range of extreme intrinsic conditions.

Blazar is a sub-category within the active galactic nuclei (AGNs) referring to sources hosting a large-scale powerful relativistic jet almost pointing in the direction of the Earth. It comprised of traditionally labelled flat spectrum radio quasars (FSRQs) and BL Lacertae objects (BLLs). Their observed continuum radiation properties are drastically different from the typical galaxies and even the non-jetted AGNs, with an almost exclusively non-thermal component dominated emission spread across the entire accessible electromagnetic (EM) windows from radio up to TeV gamma-rays (e.g. [7, 8]). The emission is characterised by a frequent and strong flux variability, strongly polarised at radio, optical, and even at X-ray in many sources (e.g. [9]) and it too varies in general with the source continuum variation (e.g. [10, 11]).

In terms of radiative output in different parts of EM windows, the broadband continuum exhibits a characteristic broad double-hump profile with a peak in near-infrared (NIR) to X-ray energies and the other at sub-MeV to GeV energies (e.g. [12]). The low-energy component spreads from radio up to X-rays and is widely considered to be the synchrotron emission from the relativistic electrons within the jet. The high-energy component, on the contrary, is still not well understood and is argued to be either due to relativistic leptons (electrons/positrons) or hadrons (protons primarily). In the lepton-based scenario, the high-energy component results from inverse Compton scattering of the surrounding photon fields while in the hadron-based explanation, it can result from proton synchrotron or an outcome of cascade triggered due to proton-proton and/or proton-photon interactions. The claim of association of neutrinos in a few blazars (e.g. [13, 14, 15]) points towards hadronic contribution but current data support minimal contribution via hadronic channels at MeV-GeV (e.g. [16]), indicating radio to GeV emission is primarily via leptonic channels.

OJ 287 is one of the most dynamic BL Lac objects located at the redshift of $z=0.306$. It is known for strong and frequent variability not only in flux/brightness but spectral and polarization as well (e.g. [17, 18, 19]). It exhibited one of the most drastic spectral variations during 2016–2017 with spectral changes in all the observational windows of the electromagnetic spectrum, especially at X-rays as reported in many previous works [20, 21, 17, 12, 22, 23, 24, 25]. Motivated by the strong X-ray spectral variation as reported in many works, argued either due to a new emission component (e.g. [17, 22, 25]) or due to the synchrotron component continuing to X-ray band (e.g. [24]). In this proceeding, we report results from the investigation of simultaneous optical to X-ray spectral variations with a focus

on the lowest optical-UV and X-ray state of the source and X-ray spectral changes.

2 Simultaneous Optical to X-ray Data

For transient and highly dynamic high-energy astronomical sources, the *Neil Gehrels Swift* observatory is the best facility for broadband observations with autonomous modes of operation capable of sampling a wide range of brightness states [26]. It hosts three astronomical payloads: the Ultra-Violet Optical Telescope (UVOT) with six astronomical filters covering optical to ultra-violet (UV) region, the X-ray Telescope (XRT) sensitive to X-ray photons of energies 0.2–10 keV, and the Burst Alert Telescope (BAT) for photons of energies between 15 to 150 keV, thereby offering simultaneous coverage from optical to hard X-ray bands of the electromagnetic spectrum. For our work here, we have used the public archival data from two of the payloads: UVOT (Ultra-violet) and XRT (X-Ray Telescope) from the start of the operation of the facility in 2005 to 2022 to study the spectral evolution of the BL Lac object OJ 287.

Except for a few pointing observations, most of the XRT observations have a typical exposure of around a kilo-second with an exposure of a few hundred seconds in a UVOT filter. Such a typical exposure is sufficient for the spectral and temporal study of OJ 287 most of the time by these instruments. The BAT is not so sensitive for temporal or spectral studies with this kind of exposure unless the source is too bright like a GRB and thus BAT is not considered (e.g. [27]).

The details of data UVOT and XRT reduction employed for this study are described in [28]. In short, for flux density extraction from the UVOT bands, a standard source region of $5''$ and an annular background region free of any source of inner and outer radii $15''$ and $20''$ was employed. For X-ray, a circular source region of $47''$ was used while the background was extracted using an annular region with inner and outer radii respectively of $65''$ and $90''$. The UVOT flux densities were then extracted using the task *wvotsource* while XRT flux points were extracted by fitting the spectra within the XSPEC [?] with an absorption-modified power-law (PL: $N(E) \equiv K(E/E_0)^{-\Gamma}$) and log-parabola model (LP: $N(E) \equiv K(E/E_0)^{-\alpha-\beta \log(E/E_0)}$). The best model out of the two was chosen based on the F-test value. For simultaneous optical-UV to X-ray spectral study, the UVOT files were converted to the respective PHA files using the HEASOFT task *wvot2pha* and the simultaneous fitting was performed in the XSPEC.

3 Analysis and Results

Figure 1 shows the simultaneous optical to X-ray light curve extracted using the pointed mode data from the XRT and UVOT between 2005 and 2022 (MJD: 53510 – 59970). In terms of variability, the XRT flux spans > 2 orders of magnitude between the recorded minimum and maximum flux in the 0.3 – 10 keV while UVOT bands during this period exhibit > 1 order of magnitude in the flux density. The strong flux changes are associated with strong spectral changes as reported in various studies (e.g. [20, 17, 22, 24]) and the 2016-2017 activity was also coincident with the first ever reported very high energy (VHE; $E > 100$ GeV) activity of the source by the VERITAS observatory [29].

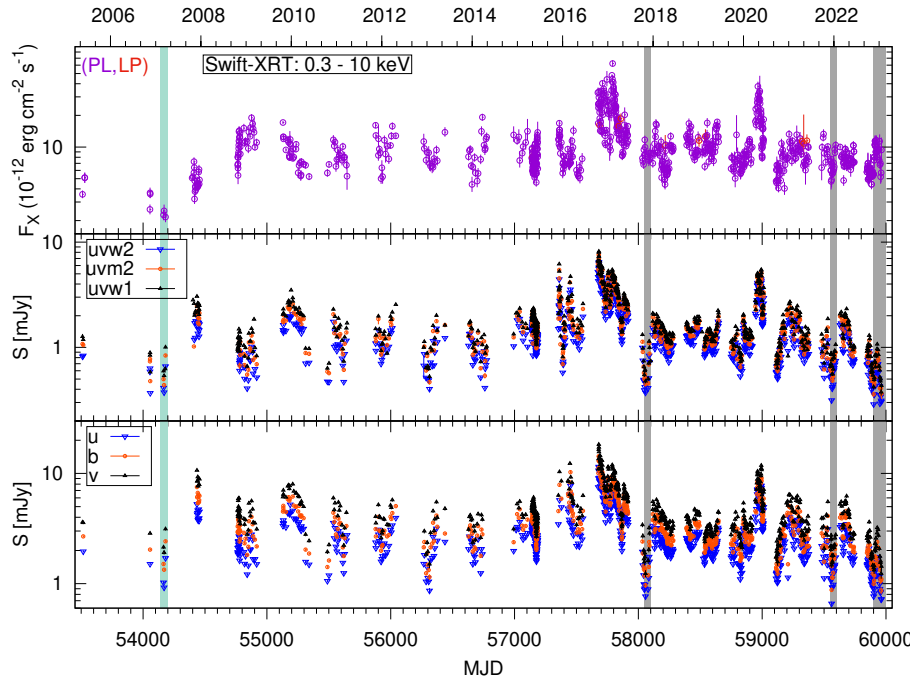


Fig. 1 Simultaneous optical to X-ray light curve of OJ 287 from the *Swift* facility observation between 2005 to 2022 (ref §2). The cyan shaded region is the focus of this work while the grey-shaded regions mark the periods with significant spectral changes in the broadband SED e.g. [20, 35, 17, 22, 24].

In terms of simultaneous flux/brightness variability trend at optical-UV and X-rays, one can observe a peculiar feature – a simultaneous low in both during MJD: 54160 – 54180. Later though optical-UV has gone even lower but not the X-rays. Since many previous studies have reported synchrotron

driving X-ray spectral changes (e.g. [24, 30, 31] and references therein), we explored the optical-UV to X-ray spectral state of the lowest optical-UV and X-ray state during this simultaneous low phase. For this, we first searched the lowest X-ray flux and then the lowest optical-UV within it, resulting in one (Obs-ID:00030901002). The details of criteria and fitting are given in [28] and the joint fitting was performed in the XPSEC using the respective source, background, response, and auxiliary files.

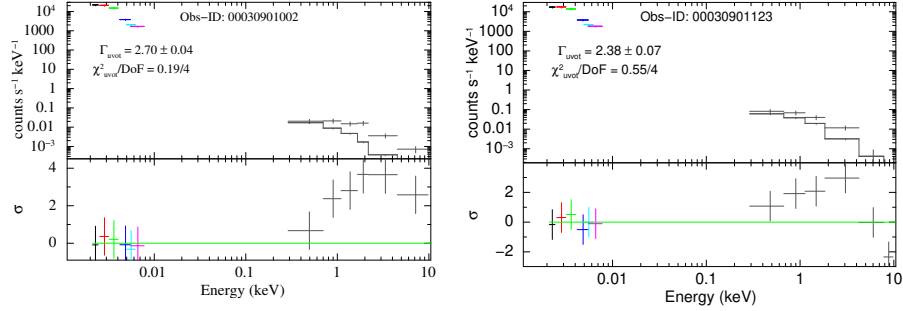


Fig. 2 The best-fit power-law optical-UV spectrum and its comparison with the X-ray data for the lowest simultaneous optical-UV and X-ray phase: Obs-ID: 00030901002, and another similar optical-UV state with a different spectral index and also a higher X-ray flux: Obs-ID: 00030901123 (see 3).

First, we independently verified the optical-UV spectrum and found it consistent with a power-law spectrum with a photon spectral index of $\Gamma_{UVOT} = 2.70 \pm 0.04$ ($\chi^2/\text{DoF} = 0.19/4$; DoF: Degree of Freedom). This best fit and its comparison with the X-ray data is shown in Figure 2 (Obs-ID:00030901002). Similarly, we independently verified the corresponding X-ray and found it consistent with a power-law with a photon spectral index of $\Gamma_X = 1.41 \pm 0.15$ ($C_{\text{stat}} = 76.9/84$). Since the optical-UV best-fit contribution at X-ray is lower/similar to X-ray data, assuming that optical-UV continues to extend to X-ray, we performed a joint-fit and got an acceptable fit with a photon spectral index of $\Gamma_{UVOT} = 2.71 \pm 0.03$ and $\Gamma_X = 1.22 \pm 0.20$. This is the hardest reported X-ray spectrum of OJ 287 to the best of our knowledge and consistent with the inferred X-ray spectrum at hard X-ray energies explored by the Swift-BAT [27]. The uncertainty is high due to low exposure leading to lower counts. However, joint modelling involving similar X-ray spectral states leads to tighter constraints consistent with the current one (e.g. see [28] for more details).

The above joint modelling and inferences were under the assumption that the power-law optical-UV synchrotron spectrum extends unhindered to X-ray energies during this simultaneous low flux state at optical-UV and X-rays. To firmly establish this, we searched other optical-UV states having similar optical-UV flux and examined the X-ray spectra. Interestingly, we

found an observation (ID:00030901123) having almost similar optical-UV flux in U-band but a very different spectrum, both at optical-UV and X-ray. We found that this different X-ray spectrum can be simply reproduced with the corresponding synchrotron and the inferred low-hard X-ray spectrum inferred for the low state as shown in Figure 3, indicating an extended optical-UV spectrum during very low optical-UV flux states.

4 Discussion

X-ray emission from OJ 287 is generally attributed to the synchrotron self-Compton (SSC) i.e. inverse Compton scattering of synchrotron photon (e.g. [31, 32]). However, many studies have also reported significant contribution of the optical-UV synchrotron high-energy tail to X-rays (e.g. [31, 24]). Without any other contamination, the SSC spectral shape is related to the spectral shape of the low-energy part of the particle distribution and the low-energy cutoff (e.g. [33, 34]).

As stated earlier, OJ 287 has shown significant X-ray spectral variability. With our focus on understanding X-ray spectral changes, especially the role of the optical-UV synchrotron component in driving these changes, we investigated the simultaneous optical-UV to X-ray variation of OJ 287 during the low optical-UV and X-ray state. Variability analysis of the light curve presented in Figure 1 shows that between 2005 and 2022 OJ 287 has exhibited drastic flux/brightness variability, by a factor of > 10 at optical-UV and even more drastic at X-ray – by a factor > 100 between the minimum and the maximum. The drastic flux variability is accompanied by an equally drastic spectral variability across the EM spectrum as reported in previous multi-wavelength studies [20, 21, 17, 12, 22, 23, 24, 25, 36]. Focussing on simultaneous¹ optical-UV and X-ray variation, we found a duration: MJD 54160-54180 (cyan-coloured band in Figure 1) having the lowest simultaneous state in both and jointly investigated the optical-UV to X-ray spectrum.

Jointly modelling the simultaneous optical-UV to X-ray spectrum of the lowest recorded X-ray flux state (see §3), we found a power-law optical-UV spectrum with $\Gamma_{UVOT} = 2.71 \pm 0.03$ extending to X-ray energies (see Figure 2-left). Accounting for this contribution at X-ray led to a very hard X-ray spectrum of $\Gamma_X = 1.22 \pm 0.20$. This inference was factually verified and firmly established with our finding of another similar low-flux optical-UV state with an altogether different optical-UV and a much brighter X-ray flux as shown in Figure 2-right. This different X-ray spectrum is naturally reproduced as the sum of its optical-UV power-law synchrotron component and the lowest inferred hard X-ray spectrum as shown in Figure 3.

¹ within the data and cadence

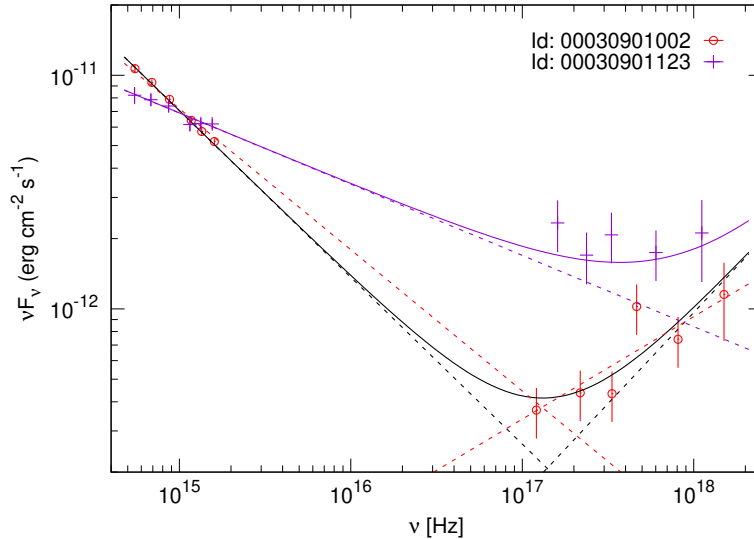


Fig. 3 The simultaneous optical-UV to X-ray SED extracted from for the lowest phase (Id: 00030901002) showing best-fit power-law shape from independent fitting (red dashed curves) and from the joint modelling (black dot-dashed curves). The purple data is the other optical-UV spectrum having almost the same UVW1-band flux along with the corresponding X-ray spectrum with curves showing independent optical-UV fit (purple dashed) and the reproduced of X-ray spectrum: purple-dashed optical-UV synchrotron + the inferred hardest X-ray spectrum during the lowest X-ray flux state (see §3).

Since the optical-UV continuum is synchrotron emission (e.g. [31, 32]) and directly traces the high-energy part of the underlying particle distribution, the finding has two direct implications as far as the X-ray spectral changes are concerned in OJ 287: (a) the optical-UV spectrum extends to X-ray energies and play significant role in driving X-ray spectral changes during low-brightness phases and (b) the underlying particle spectrum governing the optical-UV synchrotron extends to much higher energies during low-brightness phases.

Since the jet plasma is very rare (collision-less), the particle acceleration and resulting spectrum are in general related to the size of confinement of the particle within the emission/acceleration region [37] and losses e.g. radiative, an extended particle spectrum indicate a much larger emission region and also a relatively much lesser radiative losses. Thus the inferred low and hard X-ray spectrum could be a persistent low-lying component which may be the large-scale jet emission. The inferred optical-UV spectrum implies a corresponding relativistic particle distribution with a power-law spectrum of 4.4 ± 0.6 . Similarly using the same relation, the inferred hard X-ray spectrum implies a particle spectrum of power-law index 1.15 – 1.3. However, it should be noted that the inferred X-ray particle spectrum may not be a true representative of the underlying particle as such a hard state can also be reproduced via

a particle distribution with a power-law index closer to the one predicted in standard shock acceleration e.g., [33, 34, 28] with a relatively higher lower energy cutoff – also consistent with a larger acceleration/emission region.

5 Summary and Conclusion

OJ 287 has exhibited drastic spectral changes at X-rays which, in general, have been attributed to SSC but optical-UV synchrotron has also been reported to affect the X-ray spectrum in many previous studies. In the quest to understand the role of the optical-UV synchrotron component in causing X-ray spectral changes, we systematically investigated the simultaneous optical-UV and X-ray variability of the source with a focus on the simultaneous low-state in both.

We found a simultaneous low optical-UV and X-ray phase and examined the lowest optical-UV to X-ray state. First, we explored the optical-UV spectrum and found it consistent with a PL spectrum. We then accessed this best-fit with the X-ray data by extrapolating the PL to X-ray and found that the lowest energy X-ray data is consistent with the best fit optical-UV spectrum. We then performed the joint fit of optical-UV to X-ray and inferred a very hard X-ray spectrum with a power-law photon index $\Gamma_X = 1.22 \pm 0.20$ – the hardest reported X-ray spectrum for OJ 287 to the best of our knowledge. We also found another observation with an almost similar UVW1 band flux but a significantly different optical-UV and X-ray spectra with a much higher X-ray flux. We showed that this X-ray spectrum can be naturally reproduced as the sum of its optical-UV PL synchrotron component and the discovered hard X-ray spectrum, establishing our assumption that optical-UV synchrotron spectrum during very low-optical-UV brightness extends to much higher energies.

The inferred lowest flux yet hard X-ray state and the corresponding optical-UV synchrotron with a high-energy tail imply a much larger acceleration region and could be a persistent emission component associated with the large-scale jet. The extended lowest-state optical-UV spectrum implies a particle distribution (high-energy part) with a power-law index of ~ 4.4 while X-ray implies the low-energy part of a power-law index of $\sim 1.15 - 1.3$. It should be noted that such a hard X-ray spectrum can be reproduced via the standard shock spectrum with a much higher low-energy cutoff in the particle spectrum and may not be reflective of an actual hard particle spectrum.

6 Acknowledgement

The author acknowledge support from the INSPIRE Faculty grant (DST/INSPIRE/04/2020/002586) from the Department of Science and Technology (DST), Government of India.

References

1. Scaringi, S., Maccarone, T. J., Kording, E., et al. 2015, *Science Advances*, 1, e1500686. doi:10.1126/sciadv.1500686
2. Kushwaha, P., Chandra, S., Misra, R., et al. 2016, *ApJ*, 822, L13. doi:10.3847/2041-8205/822/1/L13
3. Kushwaha, P., Sinha, A., Misra, R., et al. 2017, *ApJ*, 849, 138. doi:10.3847/1538-4357/aa8ef5
4. Burke, C. J., Shen, Y., Blaes, O., et al. 2021, *Science*, 373, 789. doi:10.1126/science.abg9933
5. Zhang, H., Yang, S., & Dai, B. 2024, *ApJ*, 967, L18. doi:10.3847/2041-8213/ad488d
6. Padovani, P. 2017, *Nature Astronomy*, 1, 0194. doi:10.1038/s41550-017-0194
7. Abdo, A. A., Ackermann, M., Agudo, I., et al. 2010, *ApJ*, 716, 30. doi:10.1088/0004-637X/716/1/30
8. Gupta, A. C., Mangalam, A., Wiita, P. J., et al. 2017, *MNRAS*, 472, 788. doi:10.1093/mnras/stx2072
9. Liodakis, I., Marscher, A. P., Agudo, I., et al. 2022, *Nature*, 611, 677. doi:10.1038/s41586-022-05338-0
10. Hazama, N., Sasada, M., Imazawa, R., et al. 2022, *PASJ*, 74, 1041. doi:10.1093/pasj/psac054
11. Gupta, A. C., Kushwaha, P., Valtonen, M. J., et al. 2023, *ApJ*, 957, L11. doi:10.3847/2041-8213/acfd2e
12. Kushwaha, P. 2022, *Journal of Astrophysics and Astronomy*, 43, 79. doi:10.1007/s12036-022-09872-1
13. IceCube Collaboration, Aartsen, M. G., Ackermann, M., et al. 2018, *Science*, 361, eaat1378. doi:10.1126/science.aat1378
14. IceCube Collaboration, Aartsen, M. G., Ackermann, M., et al. 2018, *Science*, 361, 147. doi:10.1126/science.aat2890
15. IceCube Collaboration, Abbasi, R., Ackermann, M., et al. 2022, *Science*, 378, 538. doi:10.1126/science.abg3395
16. Gao, S., Fedynitch, A., Winter, W., et al. 2019, *Nature Astronomy*, 3, 88. doi:10.1038/s41550-018-0610-1
17. Kushwaha, P., Gupta, A. C., Wiita, P. J., et al. 2018, *MNRAS*, 479, 1672. doi:10.1093/mnras/sty1499
18. Gupta, A. C., Gaur, H., Wiita, P. J., et al. 2019, *AJ*, 157, 95. doi:10.3847/1538-3881/aafe7d
19. Komossa, S., Grupe, D., Kraus, A., et al. 2022, *MNRAS*, 513, 3165. doi:10.1093/mnras/stac792
20. Komossa, S., Grupe, D., Schartel, N., et al. 2017, *New Frontiers in Black Hole Astrophysics*, 324, 168. doi:10.1017/S1743921317001648
21. Komossa, S., Grupe, D., Parker, M. L., et al. 2021, *MNRAS*, 504, 5575. doi:10.1093/mnras/stab1223
22. Kushwaha, P., Pal, M., Kalita, N., et al. 2021, *ApJ*, 921, 18. doi:10.3847/1538-4357/ac19b8

23. Kapanadze, B., Vercellone, S., Romano, P., et al. 2018, *MNRAS*, 480, 407. doi:10.1093/mnras/sty1803
24. Singh, K. P., Kushwaha, P., Sinha, A., et al. 2022, *MNRAS*, 509, 2696. doi:10.1093/mnras/stab3161
25. Huang, S., Hu, S., Yin, H., et al. 2021, *ApJ*, 920, 12. doi:10.3847/1538-4357/ac0eff
26. Gehrels, N., Chincarini, G., Giommi, P., et al. 2004, *ApJ*, 611, 1005. doi:10.1086/422091
27. Langejahn, M., Kadler, M., Wilms, J., et al. 2020, *A&A*, 637, A55. doi:10.1051/0004-6361/202037469
28. Kushwaha, P. 2023, arXiv:2305.16144. doi:10.48550/arXiv.2305.16144
29. Brien, S. O. & VERITAS Collaboration 2017, 35th International Cosmic Ray Conference (ICRC2017), 301, 650. doi:10.22323/1.301.0650
30. Pal, M., Kushwaha, P., Dewangan, G. C., et al. 2020, *ApJ*, 890, 47. doi:10.3847/1538-4357/ab65ee
31. Isobe, N., Tashiro, M., Sugiho, M., et al. 2001, *PASJ*, 53, 79. doi:10.1093/pasj/53.1.79
32. Kushwaha, P., Sahayanathan, S., & Singh, K. P. 2013, *MNRAS*, 433, 2380. doi:10.1093/mnras/stt904
33. Inoue, S. & Takahara, F. 1996, *ApJ*, 463, 555. doi:10.1086/177270
34. Katarzyński, K., Ghisellini, G., Tavecchio, F., et al. 2006, *MNRAS*, 368, L52. doi:10.1111/j.1745-3933.2006.00156.x
35. Kushwaha, P., Gupta, A. C., Wiita, P. J., et al. 2018, *MNRAS*, 473, 1145. doi:10.1093/mnras/stx2394
36. Prince, R., Agarwal, A., Gupta, N., et al. 2021, *A&A*, 654, A38. doi:10.1051/0004-6361/202140708
37. Hillas, A. M. 1984, *ARA&A*, 22, 425. doi:10.1146/annurev.aa.22.090184.002233